the cubic phase applies at high temperatures, *i.e.* the presence of φ_1 microdomains is not an artefact produced during cooling.

The point would be decided by a high-temperature (> 1500 K) diffraction experiment to see if the diffuse scattering was still present. This was carried out recently by Neder, Frey & Schulz (1990), who show that for single crystals of $Ca_{0.15}Zr_{0.85}O_{1.85}$ at 1550 K, diffuse neutron scattering indeed occurs, and differs little from that observed at room temperature.

References

ALLPRESS, J. G. & ROSSELL, H. J. (1975). *J. Solid State Chem.* **15**, 68–78.

ALLPRESS, J. G., ROSSELL, H. J. & SCOTT, H. G. (1974). *Mater. Res. Bull.* **9**, 455–468.

ALLPRESS, J. G., ROSSELL, H. J. & SCOTT, H. G. (1975). *J. Solid State Chem.* **14**, 264–273.

CARTER, R. E. & ROTH, W. L. (1968). *Electromotive Force Measurements in High Temperature Systems*, edited by C. B. ALCOCK, pp. 125–144. London: Institute of Mining and Metallurgy.

COWLEY, J. M. & MOODIE, A. F. (1960). *Proc. Phys. Soc.* **76**, 378–384.

DWIVEDI, A. & CORMACK, A. N. (1990). *Philos. Mag. A*, **61**, 1 62.

ETSELL, T. H. & FLENGAS, S. N. (1970). *Chem. Rev.* **20**, 339 376.

FILATOV, S. K. & FRANK-KAMENETSKII, V. A. (1969). *Kristallografiya*, **14**, 505–506.

HELLMANN, J. R. & STUBICAN, V. S. (1983). *J. Am. Ceram. Soc.* **66**, 260–264.

LEVIN, E. M. & McMURDIE, H. F. (1975). *Phase Diagrams for Ceramists*. Columbus, Ohio: American Ceramic Society.

MICHEL, D. (1973). *Mater. Res. Bull.* **8**, 943–950.

MORINAGA, M., COHEN, J. B. & FABER, J. JR (1979). *Acta Cryst.* A35, 789–795.

MORINAGA, M., COHEN, J. B. & FABER, J. JR (1980). *Acta Cryst.* A36, 520–530.

NEDER, R. B., FREY, F. & SCHULZ, H. (1990). *Acta Cryst.* A46, 799–809.

O'KEEFE, M. A. & BUSECK, P. R. (1979). *Trans. Am. Crystallogr. Assoc.* **15**, 27–46.

ROSSELL, H. J. (1981). *Science and Technology of Zirconia, Advances in Ceramics*, edited by A. H. HEUER & L. W. HOBBS, Vol. 3, pp. 47–63. Columbus, Ohio: American Ceramic Society.

ROSSELL, H. J., SELLAR, J. R. & WILSON, I. J. (1986). *Electron Microscopy*, Vol. 2. In *J. Electron Microsc.* **35**(Suppl.), 1667–1668.

SHIOJIRI, M., HIROTA, Y., ISSHIKI, T., MAEDA, T. & SEKIMOTO, S. (1988). *Thin Solid Films*, **162**, 235–246.

WILSON, I. J. (1985). *Opt. Acta*, **32**, 1497–1507.

Structure Refinement of Commensurately Modulated Bismuth Tungstate, Bi_2WO_6

BY A. DAVID RAE

School of Chemistry, University of New South Wales, PO Box 1, Kensington, New South Wales 2033, Australia

AND JOHN G. THOMPSON AND RAY L. WITHERS

Research School of Chemistry, Australian National University, GPO Box 4, Canberra, ACT 2601, Australia

Abstract

The displacive ferroelectric Bi_2WO_6 [$M_r = 697.81$, $a = 5.4559$ (4), $b = 5.4360$ (4), $c = 16.4298$ (17) Å, $Z = 4$, $D_x = 9.512$ g cm^{-3}, Mo $K\alpha$, $\lambda = 0.7107$ Å, $\mu = 958.6$ cm^{-1}, $F(000) = 1151.73$], is described at room temperature as a commensurate modulation of an idealized $Fmmm$ parent structure derived from an $I4/mmm$ structure. Transmission electron microscopy clearly showed that there are coherent intergrowths of two distinct modulated variants in Bi_2WO_6 crystals. Displacive modes of inherent $F2mm$ and $Bmab$ symmetry are substantial and coherent over a large volume. They reduce the space-group symmetry to $B2ab$. A further substantial displacive mode corresponds to rotation of corner-connected WO_6 octahedra about axes parallel to c and has either of two inherent symmetries, $Abam$ or $Bbam$, the difference being associated with the way this mode propagates along c. The dominant $Abam$ mode reduces the space-group symmetry to $P2_1ab$, while the existence of the $Bbam$ mode reduces the intensity of $h + l = 2n + 1$ data and acts like a stacking fault. Group theoretical analysis of the problem details how the X-ray data can be classified so as to monitor the refinement. Anomalous dispersion selects the overall

sign of the $F2mm$ mode and determines the polarity. The overall signs chosen for the $Bmab$ and $Abam$ symmetry components of atom displacements select between equivalent origins. The overall signs of induced modes of inherent $Amam$, $Bbab$ and $Ccma$ symmetry had to be determined by comparative refinement since the assumption that calculated phases are best estimates can retain the initial overall sign choice for these modes during least-squares refinement. Correlations between the dominant modes and the induced modes allowed a meaningful choice of signs to resolve the pseudo homometry. Only the sign of the $Bbab$ mode was capable of self-correction during refinement. A further induced mode of inherent $Cmma$ symmetry was constrained to have zero amplitude because it required the interaction of three, rather than two, of the dominant modes for its induction. A final value of $0\cdot037$ for R_1 = $\Sigma_{\mathbf{h}}||F_{obs}(\mathbf{h})| - F_{calc}(\mathbf{h})|/\Sigma_{\mathbf{h}}|F_{obs}(\mathbf{h})|$ was obtained for 2351 unmerged data with $I(\mathbf{h}) > 3\sigma[I(\mathbf{h})]$.

Introduction

Bi_2WO_6 is a member of the family of Aurivillius phases, $Bi_2O_2.A_{n-1}B_nO_{3n+1}$, many of which are displacive ferroelectrics and can be described in terms of relatively small amplitude displacive perturbations away from an $I4/mmm$ prototype parent structure (see Fig. 1). Recently we have re-refined the crystal structures of $Bi_4Ti_3O_{12}$ (Rae, Thompson, Withers & Willis, 1990) and Bi_3TiNbO_9 (Thompson, Rae, Withers & Craig, 1991). Careful analysis using improved data sets and a modulated structure approach for these two commensurate structures produced structural models substantially different from those previously reported (Dorrian, Newnham, Smith & Kay, 1971; Wolfe, Newnham, Smith & Kay, 1971). Apart from these two members, the crystal structures of only two other members have been

determined, namely Bi_2WO_6 (Wolfe, Newnham & Kay, 1969) and $Bi_2(Sr_{0.9}Ba_{0.1})Ta_2O_9$ (Newnham, Wolfe, Horsey, Diaz-Colon & Kay, 1973).

As the reported structure of Bi_2WO_6 was determined from relatively few (16) intensities derived from neutron powder diffraction, and as the earlier crystal structure refinements of $Bi_4Ti_3O_{12}$ and Bi_3TiNbO_9 both subsequently proved to have fallen into false minima, it was deemed important that the crystal structure of Bi_2WO_6 be re-refined also. Furthermore, preliminary apparent valence calculations of the refined structure of Wolfe et al. (1969) indicated that their model was highly improbable. In particular their space-group assignment of $B2cb$ precluded the rotation of WO_6 octahedra around axes parallel to $\mathbf{c}$ and this was an essential feature of our other refinements. For this reason we decided to re-refine the crystal structure of Bi_2WO_6 using X-ray diffraction data from a single crystal, with a parallel TEM study to assist in determining the space-group symmetry of the same material.

Although commensurately modulated structures are capable of being described and refined using standard single-atom parameters, there are distinct advantages in using the modulated-structure approach, especially when trying to understand problems in refinement. A consequence of the use of the modulated-structure approach is the desirability of simply selecting symmetry operations of the parent structure to describe true structures without further transformation of axes or origin to complicate the relationships between related structures. An a glide perpendicular to $\mathbf{b}$ is a feature of all the structures under consideration and relates atoms in linked planes of atoms perpendicular to $\mathbf{c}$. We have incorporated this feature in all space-group labels, noting that $B2cb$ is an alternate label to $B2ab$.
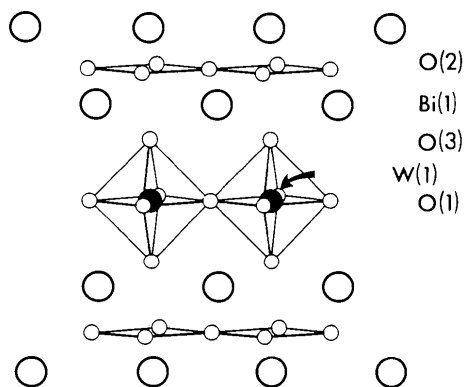

Fig. 1. A perspective drawing, approximately down $\langle 110 \rangle$, of the undistorted $Fmmm$ parent structure of Bi_2WO_6. Only atoms between $\frac{1}{4}\mathbf{c}$ and $\frac{3}{4}\mathbf{c}$ are shown.

The existence of false minima in the X-ray refinement of Aurivillius phases

We can use coefficients A_{pq} derived from the irreducible representations of the symmetry operations of a parent structure to describe the true scattering density as $\rho(\mathbf{r}) = \Sigma_p\rho_p(\mathbf{r})$ where the pth symmetrized component of the scattering density is obtained as $\rho_p(\mathbf{r}) = \Sigma_q A_{pq}\rho(\mathbf{R}_q\mathbf{r})/N_p$ where $N_p = \Sigma_q|A_{pq}|^2$ and $\mathbf{R}_q = (\mathbf{T}_q,\mathbf{t}_q)$ is the qth of N_sN_c symmetry operations of the parent structure where $\mathbf{R}_q\mathbf{r} = \mathbf{T}_q\mathbf{r} + \mathbf{t}_q$. N_s is the number of symmetry operations per unit cell and N_c is the number of unit cells in the crystal. The Fourier transform of the scattering density is then described as

$$F(\mathbf{h}) = \Sigma_p F_p(\mathbf{h}) \qquad (1)$$

where $F_p(\mathbf{h})$ is the Fourier transform of $\rho_p(\mathbf{r})$.

Group theory (Bradley & Cracknell, 1972) may be used to select the coefficients A_{pq}. The pth set of coefficients is associated with a particular vector k_p in the Brillouin zone of the parent structure and A_{pq} $= \exp(-ik_p.t_q)X_n(T_q)$ for a particular n. For a particular h in (1) the summations need only be over those selections of p for which $h = g + k_p$ where g is a Bragg reflection of the parent structure. The orthogonality of irreducible representations gives:

$$\sum_q F(T_q^{-1}h)|^2/N_q = \sum_p F_p(h)^2 \qquad (2)$$

where N_q is the number of pseudo-equivalent reflections with intensities $|F(T_q^{-1}h)|^2$.

In the case of the Aurivillius phases $T_q^{-1}h = g + k_p$ holds for all symmetry operations of the parent structure of $Fmmm$ symmetry when considering the allowed Brillouin-zone points k_p and the coefficients $X_n(T_q)$ are the same as those of the mmm point group and are listed in Table 1. The irreducible representations have been labelled according to the space group that would result should only symmetry elements with $A_{pq} = 1$ be used.

Eight irreducible representations are possible for each k_p but only two of these may be used to describe modulations within the constraint of non-centrosymmetric orthorhombic symmetry. In this instance the orthogonality relationship above reduces to

$$[|F(h)|^2 + |F(-h)|^2]/2 = |F_{p'}(h)|^2 + F_{p''}(h)|^2. \qquad (3)$$

In the absence of anomalous dispersion Friedel's Law applies and $|F(h)|^2 = |F(-h)|^2$ so that equation (3) becomes

$$|F(h)|^2 = |F_{p'}(h)|^2 + |F_{p''}(h)|^2. \qquad (3')$$

A further two irreducible representatives are associated with each point and its pseudo equivalents if the symmetry is reduced to monoclinic. Problems in structure refinement occur when certain $F_p(h)$ components dominate intensity measurements relative to other components. This can be restated in terms of the scattering density components $\rho_p(r)$ which can be said to potentially have problems of scale, sign (± 1) and structure definition.

The relative signs of the components $\rho_p(r)$ are associated with choices of origin and orientation of the crystal structure, but this need not eliminate all choice. The sign choice for the $Fmmm$ component $\rho_1(r)$ selects between 0,0,0 and $\frac{1}{2},\frac{1}{2},\frac{1}{2}$ as the origin of the parent structure model. The sign of the $F2mm$ component $\rho_2(r)$ determines the direction of the polarity of the crystal, but this can only be determined by data refinement when anomalous scattering atoms are present. A major cause of difficulty in structure refinement is the $F2mm$ component since the data has to be good enough for this component to be reliable since it and the dominant

Table 1. *The irreducible representations of Fmmm associated with the* $k = a^*$, $k = b^*$, $k = c^*$, $k = 0$ *points of the Brillouin zone and their effective space-group labels* (*space group corresponding to the symmetry operation with characters of* $+1$)

Only the symmetry elements with a zero translational component are listed.

1	2_x	2_y	2_z	-1	m_x	m_y	m_z	$k = a^*$	$k = b^*$	$k = c^*$	$k = 0$
X_1	$+1$	$+1$	$+1$	$+1$	$+1$	$+1$	$+1$	$+1$	$Ammm$	$Bmmm$	$Cmmm$	$Fmmm$
X_2	$+1$	$+1$	-1	-1	$+1$	$+1$	-1	-1	$Amaa$	$Bmab$	$Cmca$	$F2/m11$
X_3	$+1$	-1	-1	$+1$	$+1$	-1	-1	$+1$	$Abam$	$Bbam$	$Cccm$	$F112/m$
X_4	$+1$	-1	$+1$	-1	$+1$	-1	$+1$	-1	$Ahma$	$Bhmb$	$Ccma$	$F12/m1$
X_5	$+1$	$+1$	$+1$	$+1$	-1	-1	-1	-1	$Abaa$	$Bbab$	$Ccca$	$F222$
X_6	$+1$	$+1$	-1	-1	-1	-1	$+1$	$+1$	$Ahmm$	$Bhmm$	$Ccmm$	$F2mm$
X_7	$+1$	-1	-1	$+1$	-1	$+1$	$+1$	-1	$Amma$	$Bmmh$	$Cmma$	$Fmm2$
X_8	$+1$	-1	$+1$	-1	-1	$+1$	-1	$+1$	$Amam$	$Bmam$	$Cmcm$	$Fm2m$

In the absence of anomalous dispersion contributions to the scattering factor from scattering density components transforming as the irreducible representations X_1 to X_4 are real while those for X_5 to X_8 are imaginary.

Multiplication tables

	X_1	X_2	X_3	X_4	X_5	X_6	X_7	X_8
X_1	X_1	X_2	X_3	X_4	X_5	X_6	X_7	X_8
X_2	X_2	X_1	X_4	X_3	X_6	X_5	X_8	X_7
X_3	X_3	X_4	X_1	X_2	X_7	X_8	X_5	X_6
X_4	X_4	X_3	X_2	X_1	X_8	X_7	X_6	X_5
X_5	X_5	X_6	X_7	X_8	X_1	X_2	X_3	X_4
X_6	X_6	X_5	X_8	X_7	X_2	X_1	X_4	X_3
X_7	X_7	X_8	X_5	X_6	X_3	X_4	X_1	X_2
X_8	X_8	X_7	X_6	X_5	X_4	X_3	X_2	X_1

	$k = a^*$	$k = b^*$	$k = c^*$	$k = 0$
$k = a^*$	$k = 0$	$k = c^*$	$k = b^*$	$k = a^*$
$k = b^*$	$k = c^*$	$k = 0$	$k = a^*$	$k = b^*$
$k = c^*$	$k = b^*$	$k = a^*$	$k = 0$	$k = c^*$
$k = 0$	$k = a^*$	$k = b^*$	$k = c^*$	$k = 0$

$Fmmm$ component are observed simultaneously. Absorption corrections have to be sufficiently accurate. The structures we have studied have $\mu = 700$–1000 cm^{-1} for Mo $K\alpha$ radiation. Accuracy can be achieved by refining the thin crystal dimension defining plate thickness using correlations from a full sphere of data and then excluding those equivalents of a reflection for which absorption was too high. Anisotropic extinction corrections are also necessary.

The anomalous dispersion has a benefit in that it creates an imaginary component of the structure factor associated with the $Fmmm$ parent structure which then correlates with the $F2mm$ component and increases the fractional contribution of the imaginary component of the structure factor to the observed intensity. Since least-squares refinement of X-ray data implicitly assumes the calculated phase of reflections is correct, the increase in reliability of the imaginary component of residuals of F-centred data is very beneficial. Displacing an oxygen atom in the wrong direction along a can be stabilized by using isotropic thermal parameters and the misbehaviour of anisotropic thermal parameters can be an indication of error rather than unrefineability (Rae,

Thompson & Withers, 1990). Refinement of occupancies at mirror-related sites also selects correct atom displacements for the $F2mm$ mode.

The distinction between 0,0,0 and $0,\frac{1}{2},\frac{1}{2}$ as the origin of a B-centred structure, e.g. bismuth titanate or a component of the bismuth tungstate structure, is determined by the selection of sign relative to $\rho_1(\mathbf{r})$ for one component, either $\rho_3(\mathbf{r})$ or $\rho_4(\mathbf{r})$, associated with the extra reflections ($\mathbf{k} = \mathbf{b}^*$). The relative sign of the fourth component creates geometrically different structures and can only be determined by correlations. Two correlations matter: (1) Correlations with anomalous scatterers. (2) Correlations caused by the modulations being described as atom displacements. Restricting ourselves to non-global parameters (i.e. excluding scale, extinction etc.) we can use a Taylor's expansion to describe the structure factor as

$$F(\mathbf{h}) = F(\mathbf{h})_o + \sum_n \sum_{rp} [\partial F(\mathbf{h}) / \partial s_{nrp}]_o \Delta s_{nrp}$$
$$+ \tfrac{1}{2!} \sum_n \sum_{rr'pp'} [\partial^2 F(\mathbf{h}) / \partial s_{nrp} \partial s_{nr'p'}]_o \Delta s_{nrp} \Delta s_{nr'p'} + \ldots$$

$$(4)$$

where $\Delta s_{nrp} = \sum_q A_{pq}{}^* \Delta \nu_{nqr} / N_p$ and inversely $\Delta \nu_{nqr} = \sum_p A_{pq} \Delta s_{nrp}$ where $\Delta \nu_{nqr}$ implies the change from the parent structure value of the rth parameter of the nth atom as manifested at the qth equivalent position of the parent structure. Δs_{nrp} is a change in the pth symmetrized combination of equivalents of the rth parameter of the nth atom. The subscript o implies evaluation using the parameters associated with the parent. Parameters Δs_{nrp} and $\Delta \nu_{nqr}$ span the same variable space.

If the only variables are occupancy parameters and $\rho(\mathbf{r})_o$ corresponds to the $p = 1$ irreducible representation in which all A_{1q} equal 1 then the above series expansion terminates after the first-order terms and for other p values, $F_p(\mathbf{h}) = \sum_{nr} [\partial F(\mathbf{h}) / \partial s_{nrp}]_o \Delta s_{nrp}$. If the only variables are for displacements of atom positions then the series is infinite as we are differentiating $\exp(i\mathbf{h}.\mathbf{r})$-type terms and the symmetry of terms in Δs_{nrp}, $\Delta s_{nrp}\Delta s_{nr'p'}$, etc. determine which $F_p(\mathbf{h})$ component is contributed to by which particular term in the series expansion. In particular, if p and p' are associated with Brillouin-zone points $\mathbf{k}$ and $\mathbf{k}'$ then the $\Delta s_{nrp}\Delta s_{nr'p'}$ term is associated with the contribution for the point $\mathbf{k} + \mathbf{k}'$. The appropriate $X_n(T_q)$ values are obtained from the multiplication of the irreducible representations and these results are also listed in Table 1. Also, terms involving $|\Delta s_{nrp}|^2$ are associated with $\mathbf{k} = 0$ and $p = 1$ since $\Delta s_{nrp}{}^*$ is associated with $-\mathbf{k}$. Thus the dominant $Fmmm$ component of the structure factors contains second-order information about the magnitudes but not phases of atom-displacement components. Consequently, the dominance of the $Fmmm$ component over the $F2mm$ component as a contri-

butor to intensity can result in incorrectly signed $F2mm$ components of displacements of individual atoms, which are stabilized if the thermal parameters are constrained to be isotropic. The inclusion of anisotropic thermal motion further complicates the picture. Thermal parameters can compensate for errors in the atom-displacement components as they simulate correlations between first-order displacive components. The occurrence of unlikely thermal parameters can be used as a diagnostic to indicate systematic error (Rae, Thompson & Withers, 1990).

Provided displacements are sufficiently small the first-order terms in the series (4) are dominant and a particular combination Δs_{nrp} is determined by a particular component of the data since $F_p(\mathbf{h})$ is approximated by $\sum_{nr} [\partial F(\mathbf{h}) / \partial s_{nrp}]_o \Delta s_{nrp}$. The apparent scale of $F_p(\mathbf{h})$ data and hence Δs_{nrp} parameters may be altered by disorder and twinning. The second-order terms in (4) are correlations and link components of the data since the irreducible representation associated with the correlation term is obtained from the product of the irreducible representations of the relevant first-order terms. However, when displacements are small these correlations make a rather small difference to refinement statistics and then only on index condition selected data.

In the case of $Bi_4Ti_3O_{12}$, refinement used standard atom parameters in a standard manner but results and reflection data were analysed using a modulated-structure approach. The only constraints were to maintain $B2ab$ symmetry for the anisotropic thermal parameters of atoms pseudo related by this symmetry. The only additional parameterization was a twinning parameter. The signs of the extra $\rho_p(\mathbf{r})$ components associated with $B1a1$ are determined by differences in magnitudes of the real and imaginary components of pseudo-equivalent reflections. This allows refinement of atom parameters away from values imposing $B2ab$ symmetry. The scale of these displacements was affected by twinning which reduced the differences between the observed intensities of twin-related reflections. Some of the b-glide absences of the $B2ab$ approximation are observed confirming that $B1a1$ is the true space group, and since these reflections are not affected by twinning, an estimate could be made of the correct scale for the extra displacive modes and thus resolve the correlation between partial twinning and overall mode magnitude.

The choice of the sign for $\rho_4(\mathbf{r})$ highlights the need for an extra physical calculation of correctness to discriminate between the resulting structures which are geometrically quite different. The change of sign for this component in bismuth titanate reduced the agreement factor $R_1 = \sum_{\mathbf{h}} |\Delta F(\mathbf{h})| / \sum |F_o(\mathbf{h})|$ from 0·027 to 0·020 before a twinning parameter further

reduced R_1 to a final value of 0·0177. Both minima were stable under anisotropic refinement because of the assumption that the phase of the observed $F(\mathbf{h})$ is that of the initial calculated estimate for least-squares refinement.

We have used apparent valence (AV) calculations (Brown, 1978, 1981; Brown & Altermatt, 1985) to distinguish the two situations clearly and independently support the final structure. These calculations also allow a method of assessing the effect of individual displacive modes singly and in concert, and will be extensively discussed elsewhere (Withers, Thompson & Rae, 1991).

Transmission electron microscopy

Electron diffraction has a proven ability to pick up weak features of reciprocal space that are often not readily detectable using conventional X-ray diffraction procedures, in particular the identification of true diffraction symmetry, the presence of weak extra reflections and the occurrence of twinning, stacking faults and intergrowths. Crushed single-crystal fragments of Bi$_2$WO$_6$ from the synthesis described below were studied in order to check the previously

reported space-group assignment of $B2cb$. Figs. 2(a–c) show typical [100], [010] and [001] zone-axis selected-area electron diffraction patterns (SADP's) while Fig. 2(d) shows a [001] zone-axis convergent-beam pattern (CBP). The strongly observed reflections largely correspond to the underlying $Fmmm$ average structure while the much weaker satellite reflections correspond to $\mathbf{k} = \mathbf{a}^*$, $\mathbf{k} = \mathbf{b}^*$ and $\mathbf{k} = \mathbf{c}^*$ displacive modulations thereof.

The weaker satellite reflections technically lower the resultant space-group symmetry to $P1a1$, $a = 5\cdot456$, $b = 5\cdot436$, $c = 16\cdot43$ Å. Note, however, the commonly observed streaking of certain classes of satellite reflections, notably the A- and C-centred classes of data ($h + l = 2n + 1$), along the $\mathbf{c}^*$ reciprocal space direction. This suggests the occurrence of some sort of planar faulting perpendicular to $\mathbf{c}^*$. This was confirmed by appropriate satellite dark-field (SDF) imaging which invariably shows an apparently coherent intergrowth of two different structures with c-axis periodicities of 16 and 8 Å respectively, see the [2$\bar{1}$0] SDF image in Fig. 3.

The structure with a 16 Å periodicity is clearly the majority phase and requires a primitive Bravais lattice. The reflections allowed to contribute to the
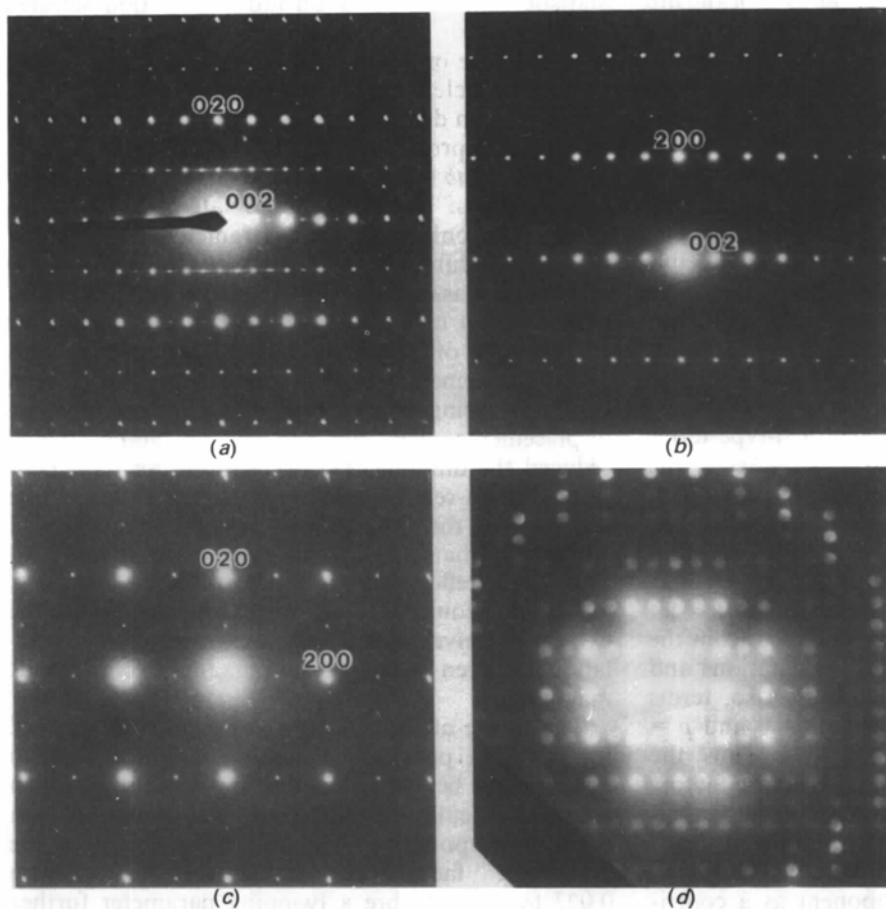

Fig. 2. Typical (a) [100], (b) [010] and (c) [001] zone-axis selected-area electron diffraction patterns. Note the streaking of the A- and C-centred classes of data in (a) and (b). (d) shows a typical [001] zone-axis convergent-beam pattern and can be indexed by reference to (c).

SDF image, see Fig. 3(b), imply the minority 8 Å phase requires a B- or A-centred Bravais lattice. Given the classes of satellite reflections for which the streaking is most pronounced, the relative strengths

(a)

(b)

Fig. 3. Typical (a) satellite dark-field (SDF) image and (b) corresponding selected-area electron diffraction pattern taken at the [2$\bar{1}$0] zone axis. The reflections allowed to contribute to the SDF image are contained between the brackets in (b). Coherent intergrowth between two distinct modulated variants is clearly visible in (a). The two distinct spacings visible are c/2 (8 Å) and c (16 Å) determined by Bravais lattices types B and P respectively. The P-centred Bravais lattice is the majority phase.

of the observed satellite reflections and a knowledge of the displacive modulations in the closely related $Bi_4Ti_3O_{12}$ (Rae, Thompson, Withers & Willis, 1990) and Bi_3TiNbO_9 (Thompson, Rae, Withers & Craig, 1991) structures, the most likely explanation is an intergrowth of a majority $P2_1ab$ structure and a minority $B1a1$ structure.

This choice of space-group options and the implicit displacement-mode description is discussed in more detail later. It is assumed that two major modulations of the $Fmmm$ parent structure, an $F2mm$ mode and a $Bmab$ mode are coherent over a large volume and create a $B2ab$ structure as an alternative parent for further modulation. This is in agreement with relative intensities and the b-glide pseudo absences (hk0 data with $k = 2n + 1$ are very weak). This component of $\rho(\mathbf{r}) = \sum_p \rho_p(\mathbf{r})$ diffracts well with no streaking. The majority $P2_1ab$ component arises predominantly from an $Abam$ displacive mode describing rotations of corner-linked planes of WO_6 octahedron about axes parallel to c. The minority $B1a1$ component arises predominantly from a $Bbam$ displacive mode. These two modes differ only in the translational arrangement relating adjacent layers of WO_6 octahedra separated by Bi_2O_2 layers perpendicular to c*. The extra reflections are streaked, but not excessively, because of the domain dimension parallel to c. Because of the much smaller domain dimension of the $B1a1$ component the contribution of $F_p(\mathbf{h})$, corresponding to the $Bbam$ mode, to $F(\mathbf{h})$ is so streaked as to be effectively a non-contributor to a normal X-ray diffraction data collection. The ability to see that the hk0 data with $k = 2n + 1$ are non-zero was a consequence of the projection of the streak down c* being observed.

Pseudo homometry in bismuth tungstate

A feature of our refinements of $Bi_4Ti_3O_{12}$ and Bi_3TiNbO_9 was that there was a choice of sign for the $\rho_2(\mathbf{r})$ and $\rho_4(\mathbf{r})$ components of the scattering density. Origin selection determined the sign of $\rho_1(\mathbf{r})$ corresponding to the $Fmmm$ average structure and $\rho_3(\mathbf{r})$ corresponding to a $Bmab$ mode in $Bi_4Ti_3O_{12}$ and an $Amam$ mode in Bi_3TiNbO_9. Comparative refinement was used to select the sign of $\rho_2(\mathbf{r})$ corresponding to the $F2mm$ displacive mode associated with the resulting ferroelectricity, and the sign of $\rho_4(\mathbf{r})$ corresponding to a $Bbab$ mode in $Bi_4Ti_3O_{12}$ and an $Abam$ mode in Bi_3TiNbO_9. Although the preferred signs agreed with the results of AV calculations the wrong sign choice for $\rho_4(\mathbf{r})$ still gave normally acceptable refinement statistics. Large anomalous dispersion allowed no doubts as to the sign of $\rho_2(\mathbf{r})$ and assisted the statistics of comparative refinement for the sign of $\rho_4(\mathbf{r})$. Poorly behaved anisotropic thermal parameters under least-squares
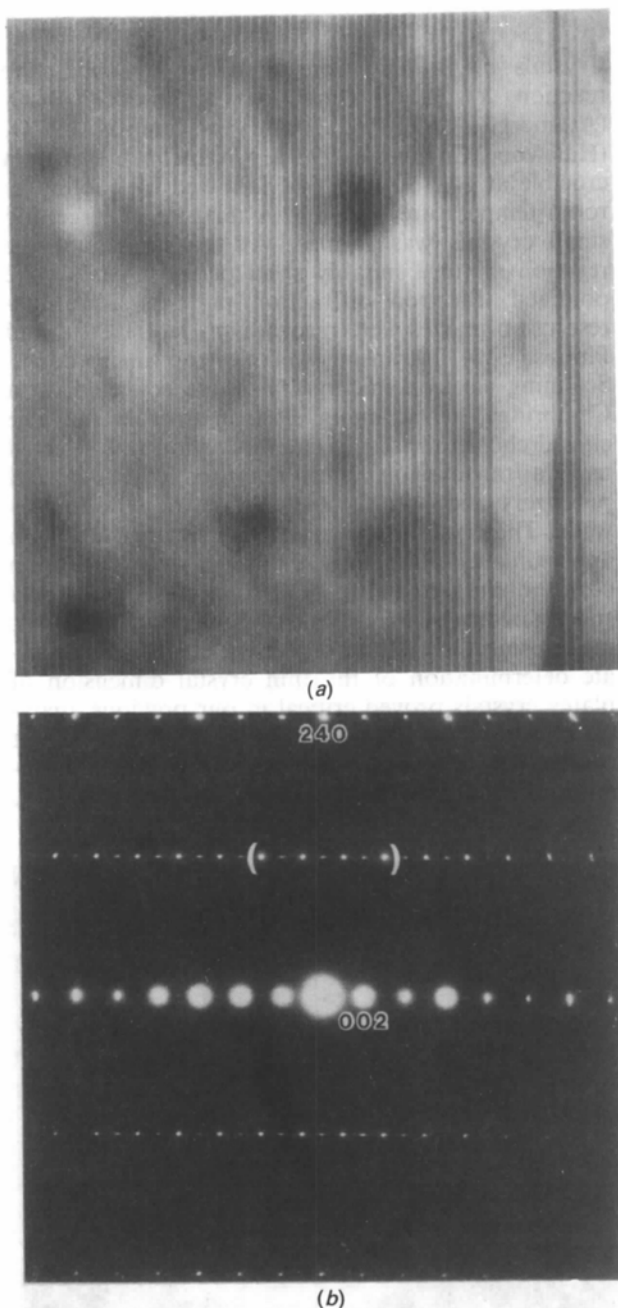
refinement were an indication of atom position error and have been previously discussed (Rae, Thompson & Withers, 1990). Four further components exist for Bi$_4$Ti$_3$O$_{12}$ associated with a reduction in symmetry to $B1a1$ and the signs for these components were determined by differences in intensities of reflections related by the loss of symmetry. Only the $Bbam$ mode was of substantial magnitude but an induced $Fmm2$ mode is associated with a small polarization component along **c**.

A pleasing feature of the refinement of Bi$_2$WO$_6$ in space group $P2_1ab$ is that the corresponding phase choices for the three major displacive modes simply define an origin choice and a choice in polarization direction which is clearly distinguished because of the high value for Bi of $\Delta f'' = 10.559$ ($\Delta f'' = 6.872$ for W) for Mo $K\alpha$ (*International Tables for X-ray Crystallography*, 1974, Vol. IV). The fact that the resulting geometrical features show an extremely good agreement with those of our preferred structures for Bi$_4$Ti$_3$O$_{12}$ and Bi$_3$TiNbO$_9$ is gratifying and suggests that our preferred structures are indeed correct.

However, there still remains four induced displacive modes permitted under $P2_1ab$ symmetry, *viz.* $Bbab$, $Amam$, $Ccma$ and $Cmma$, and for each there is a choice of sign for the corresponding $\rho_p(\mathbf{r})$ component. The true scattering density is described in terms of atoms and not $\rho_p(\mathbf{r})$ components, and displacive modes are described in terms of atom displacements. As a consequence the Taylor series (4) contains higher-order terms capable of resolving the sign problem. Individual terms apply specifically to specific hkl index conditions and the effect of these terms can be quite small if displacements are small. The assumption that the phase of the observed reflections is the same as that of an initial estimate preserves the sign of initial displacement parameters unless anomalous-dispersion components or the second-order terms of the Taylor expansion involving correctly described modes are sufficiently large to overcome this problem. These second-order terms can only arise from sizeable displacements of different symmetry involving the same atom.

Self correction proved not to be the case except for the $Bbab$ mode. This is because the anomalous dispersion associated with the Bi atoms involved in the $Bmab$ mode was large enough to dominate the imaginary component of the B-centred data. Switching the overall sign of a displacement of any of the remaining symmetries produced stable minima. It is wise to check both options even though it is possible to expand a displacement mode from zero amplitude because there is some phase information from anomalous dispersion and the second-order terms. However, this information more reliably selects between options. If this discrimination had been absent the structures would have been truly homometric as indistinguishable intensities would have produced indistinguishable Patterson (interatomic vector) maps.

Experimental

Crystals of Bi$_2$WO$_6$ were prepared by solid-state reaction of a mixture of 52.5 mol% Bi$_2$O$_3$ (Atomergic, 99.999%) and 47.5 mol% WO$_3$ (Halewood Chemicals, 99.9%) in an open platinum crucible at 1443 K for 16 h, followed by cooling to room temperature over 8 h. A mixture of large and small crystals was formed. At the surface of the reaction mixture suitably sized platey crystals were obtained. Electron diffraction patterns and high-resolution images were recorded on Jeol 100CX and Philips EM430 transmission electron microscopes. Scanning electron micrographs were collected on a Cambridge 360 scanning electron microscope. The crystal chosen for X-ray data collection was selected using a transmission optical microscope with crossed polarizers and was completely free of 90° domain walls. The crystal approximated a square plate with approximate dimensions $0.071 \times 0.105 \times 0.023$ mm corresponding to ($\bar{1}10$), (110) and (001) reciprocal space directions. Precise measurements of faces was made using the method of Alcock (1970). An accurate determination of the thin crystal dimension of platey crystals proved critical in our previous analyses of Aurivillius phases and an accurate assessment of the thin dimension was obtained using the minimum of a data merge statistic *versus* thickness plot.
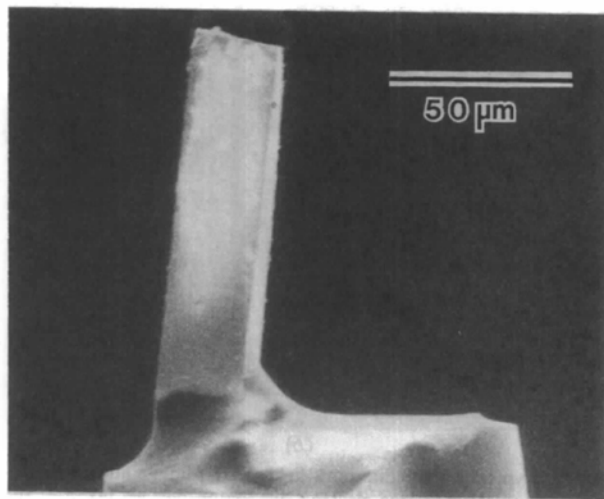

Fig. 4. Scanning electron microscope secondary-electron image of the Bi$_2$WO$_6$ crystal used for data collection still mounted on the quartz fibre. The (001) face is on the left and the (110) face at the top. This accurate measurement of thickness confirmed the value of 23.0 ± 0.4 μm obtained by data correlation. This precision is not obtainable optically.

To obtain meaningful results it was found necessary to exclude $\sin\theta/\lambda < 0.2$ Å^{-1} data from the statistics. These data were later found to suffer from anisotropic extinction. The principal axes of the later-determined type 2 parameters (Coppens & Hamilton, 1970) did not align with the crystal axes and destroyed equivalence of extinction-affected data. Dimensions used for the absorption correction were (0,0,1) and (0,0,$-$1) 0.0115 (2), ($-$1,1,0) and (1,$-$1,0) 0.0354 (5), (1,1,0) and ($-$1,$-$1,0) 0.0525 (8) and (100,138,295) 0.040 (5) mm. The optical and refinement determined dimensions were verified by measurement in the scanning electron microscope, see Fig. 4. A full sphere of Mo $K\alpha$ data (5784 primitive monochromator data) out to $\theta = 30°$ was recorded on a Philips four-circle automated diffractometer at 1° min^{-1} for a scan width of 1.3° with backgrounds of 10 s per side. The analytical absorption correction of de Meulenaer & Tompa (1965) was used, $\mu = 958.6$ cm^{-1}. Scattering curves, atomic absorption coefficients and anomalous-dispersion corrections were from International Tables for X-ray Crystallography (1974, Vol. IV).

Values of $wR = [\sum_{\mathbf{h}}N_{\mathbf{h}}\sum_i w_{\mathbf{h}i}(|F(\mathbf{h}_i)| - |F(\mathbf{h})|)^2 / \sum_{\mathbf{h}}(N_{\mathbf{h}} - 1)\sum_i w_{\mathbf{h}i}|F(\mathbf{h})|^2]^{1/2}$, where $N_{\mathbf{h}}$ is the number of independent observations of $F(\mathbf{h})|^2$, were obtained using SHELX (Sheldrick, 1976) and gave the following results for the merging of data of different index condition.

Data used	$m11$	$1m1$	$11m$
		wR(merge)	
All reflections	0.0497	0.0417	0.0525
(Absorption uncorrected)	0.1768	0.1697	0.0674
$\sin\theta/\lambda > 0.2$ Å^{-1}	0.0501	0.0427	0.0371
$\sin\theta/\lambda < 0.2$ Å^{-1}	0.0470	0.0328	0.1218

Selection of data

During refinement anisotropic secondary-extinction corrections were necessary and as a consequence unmerged data had to be used. A 2% error in $F(\mathbf{h})$ was an arbitrary addition to the counting statistic error in order to match the goodness of fit of different data classes. Refinement used 2351 data with $I(\mathbf{h}) > 3\sigma[I(\mathbf{h})]$. The overall range of transmission factors (T) was 0.013 to 0.125 but 137 reflection data with $T < 0.035$ were excluded because it was considered that the absorption correction was too unreliable, changing too rapidly with thickness. These, however, were monitored to assess the quality of the absorption correction. An additional 37 reflections were considered unobserved and excluded from refinement despite just meeting the intensity requirement. This was based on their small calculated intensity and the fact that they had more than one equivalent truly unobserved by the intensity criterion. The extra 2866 truly weak data were monitored and refined to a goodness of fit of 0.98, see Table 2. Data were

Table 2. Final refinement statistics for Bi_2WO_6

Data set	R_1	wR	G.o.f.
All 2351 used data	0.0370	0.0453	1.49
(1) 1335 eee and ooo data	0.0331	0.0417	1.55
(2) 803 eoe and oeo data	0.0426	0.0440	1.26
(3) 186 oee and eoo data	0.1145	0.1949	1.92
(4) 27 eeo and ooe data	0.0947	0.1178	0.88
(5) 137 high-absorption data	0.0563	0.0661	2.00
(6) 40 $\sin\theta/\lambda < 0.2$ Å^{-1} data	0.0681	0.0723	2.81
(7) 2866 $I < 3\sigma(I)$ data	0.585	0.400	0.98

Notes: $R_1 = \sum_{\mathbf{h}}||F_{obs}(\mathbf{h})| - F_{calc}(\mathbf{h})| / \sum_{\mathbf{h}} F_{obs}(\mathbf{h})|$,
$wR = [\sum_{\mathbf{h}}w_{\mathbf{h}}(|F_{obs}(\mathbf{h})| - F_{calc}(\mathbf{h})|)^2 / \sum_{\mathbf{h}}w_{\mathbf{h}} F_{obs}(\mathbf{h})|^2]^{1/2}$,
G.o.f. $= [\sum_{\mathbf{h}}w_{\mathbf{h}}(|F_{obs}(\mathbf{h})| - F_{calc}(\mathbf{h})|)^2 / (n - m)]^{1/2}$.

monitored by segmenting according to index, viz. h,k,l odd (o) or even (e). The 2351 used data contained 1335 F-centred $(eee$ and $ooo)$ data, 803 B-centred $(eoe$ and $oeo)$ data, but only 186 A-centred $(oee$ and $eoo)$ data and 27 C-centred $(eeo$ and $ooe)$ data. Final refinement statistics are given in Table 2.

Refinement of the structure of Bi_2WO_6

The structure was refined in space group $P2_1ab$ using the program RAELS89 (Rae, 1989). Which atom displacements contribute to which modulations is described by the results listed in Table 6. The symmetry of the modulations and their essential nature are listed in Table 3. Initial refinement only allowed refinement within the constraint that the $Bbab$, $Amam$, $Ccma$ and $Cmma$ displacive modes had zero amplitude. The overall signs for the remaining modes are simply origin and polarity choosing and the comparison between polarity options was clearly significant in the first cycle. The Bi atoms had their x values fixed at zero to define the origin in the $\mathbf{a}$ direction and the W atom was displaced ±0.5 Å to create the initial contribution to the $F2mm$ mode. O atoms were started at their $Fmmm$ parent symmetry imposed positions. The Bi atoms were displaced to create initial information for the $Bmab$ mode and the WO_6 octahedra were rotated to move O(1) and O(1') in the xy plane to create initial information for the $Abam$ mode. A single scale constant was used for all data. Anisotropic thermal parameters were used with constraints that maintained the parent structure 2_x symmetry relationship relating primed and unprimed atoms which become inequivalent once the symmetry is lowered below $B2ab$. Refinement was well behaved and converged in a few cycles. The O(1)- and O(1')-atom thermal parameters always tended to go non-positive definite and as a consequence $U_{11} = U_{22}$ was imposed as a constraint for these atoms. The sign of the $Amam$ mode was then ascertained by comparative refinement using a y displacement of the W atom to initiate the refinement options. The sign of the $Bbab$ mode was then ascertained initiated by the y displacements of the O(2) and O(2') atoms which are

Table 3. *Major and minor displacive modes for the commensurately modulated structures of three Aurivillius phases* $Bi_2O_2.A_{n-1}B_nO_{3n+1}$

n	Compound	Space group	Major components		Minor components	
3	$Bi_4Ti_3O_{12}$	$B1a1$	$F2mm$	$Bmab$	$Fmm2$	$F12/m1$
			$Bbab$	$Bbam$	$Bmam$	
2	Bi_3TiNbO_9	$A2_1am$	$F2mm$	$Abam$		
			$Amam$			
1	Bi_2WO_6	$P2_1ab$	$F2mm$	$Bmab$	$Bhab$	$Amam$
			$Abam$		$Ccma$	$(Cmma)$
		or				
		$B1a1$	$F2mm$	$Bmab$	$Bhab$	$Bmam$
			$Bbam$		$F12/m1$	$(Fmm2)$

Description of major modes of displacement

Ferroelectricity along a direction	$F2mm$	for $n = 3, 2, 1$
Alternating rotations of octahedra	$Bmab$	for $n = 3, 1$
about axes parallel to a	$Amam$	for $n = 2$
Rotation of octahedra about axes	$Bbab, Bbam$	for $n = 3$
parallel to c	$Abam$	for $n = 2$
	$Abam$ or $Bbam$	for $n = 1$

Notes: Minor displacive components can be regarded as being induced by major components.

$n = 3$ $Fmm2 = Bbab*Bbam$ $F12/m1 = Bmab*Bbam$
   $Bmam = F2mm*Bbam$
$n = 1$ $Bbab = F2mm*Bmab$ $Amam = F2mm*Abam$
   $Ccma = Abam*Bmab$ $(Cmma = F2mm*Abam*Bmab)$
or $Bbab = F2mm*Bmab$ $Bmam = F2mm*Bbam$
   $F12/m1 = Bbam*Bmab$ $(Fmm2 = F2mm*Bbam*Bmab)$

$Bbam$ mode for $n = 3$ reduces space-group symmetry from $B2ab$ to $B1a1$. This mode allows octahedron at $z = 0$ and $\frac{1}{2}$ to rotate about c. The $Bbab$ mode has anti-mirror symmetry across the $z = 0$ and $\frac{1}{2}$ planes.

the only contributions to this mode. It was found that the anomalous dispersion of Bi atoms involved in the $Bmab$ mode was sufficiently dominant to correct the wrong choice of sign for the $Bbab$ mode. The weak C-centred (eeo and ooe) data were excluded from all refinements up to this point.

The minor displacive modes can be regarded as being induced by the major $F2mm$, $Bmab$ and $Abam$ displacive modes. The multiplication of irreducible representations associated with this are given in Table 3. It is to be noted that, whereas the $Ccma$ mode can be induced using just two major modes, all three are required to induce a $Cmma$ mode. It was therefore decided to initially refine just the $Ccma$ mode and determine its choice of sign. An equal but opposite signed x displacement of the $Bi(1)$ and $Bi(1')$ ions initiates this refinement. The success of this refinement step and the paucity of the data precluded any meaningful assessment of the $Cmma$ mode which was therefore assumed to have zero amplitude.

Mindful of the comparative misbehaviour of the thermal motion of the $O(1)$ and $O(1')$ atoms consistent with an error in the scale of the A- and C-centred data and the explanation for such behaviour inherent in the SDF (Fig. 3) it was decided to refine two scale

constants, one for F- and B-centred data and a hopefully smaller one for A- and C-centred data. To counter the correlation between the scale of $O(1)$- and $O(1')$-atom displacements in the xy plane, the second scale constant and the apparent thermal motion, the minima was chosen to be that defined by the constraint that $U_{11} = U_{22}$ for these atoms.

Comparative refinement checks were then re-run for the sign options with the following discriminations between stable minima. A difference between $R_1 = 0.171$ and 0.114 (oee and eeo data only) was found for the $Amam$ mode, and between 0.143 and 0.095 (eeo and ooe data only) for the $Ccma$ mode.

A final scale ratio of $K_1(h + l = 2n + 1)/K_2(h + l = 2n) = 0.97$ (7) was obtained for $F(h)$ data. There would appear to be little of the $B1a1$ intergrowth in the crystal, but correlation problems have placed a very large error on the scale of K_1 so this result cannot be conclusive. An anisotropic extinction parameter of type 2 as described by Coppens & Hamilton (1970) was refined. The final refinement cycle data with $\sin\theta/\lambda < 0.2$ Å^{-1} had a value for R_1 of 0.068. Values of $W'_{11} = 17$ (2), $W'_{22} = 27$ (3), $W'_{33} = 27$ (4), $W'_{12} = 10$ (2) were obtained. The remaining parameters W'_{13} and W'_{23} were found to approximate zero and were subsequently constrained to be so.

Structure description

Table 4 gives the final atomic fractional coordinates and Table 5 the final anisotropic thermal parameters.* Table 6 contains a resolution of atomic parameters into the displacement modes of different symmetry. Table 7 gives the geometry of the W and Bi environments in Bi_2WO_6.

Fig. 5 shows the atom displacements corresponding to the $Bmab$ component, being the rotation of the WO_6 octahedron about the a axis, and Fig. 7 shows the atom displacements corresponding to the $Abam$ component, being the rotation of the WO_6 octahedron about the c axis (see Table 6). This latter motion, which is precluded by the space group $B2ab$, has a significant magnitude and involves a $9.0°$ rotation of the octahedron from its high-symmetry parent position.

Both of these octahedral rotations were also observed in our previous refinements of $Bi_4Ti_3O_{12}$ and Bi_3TiNbO_9. Furthermore, the magnitudes of the atom displacements associated with these motions are so similar as to be almost identical.

The other major displacive component in Bi_2WO_6 is the 'ferroelectric' $F2mm$ component (Table 6 and

Table 4. *Fractional coordinates for* Bi_2WO_6 ($\times 10^4$)

	x	y	z^*
W(1)	209 (1)	79 (5)	5000
Bi(1)	40 (4)†	4810 (1)	6723 (0)
Bi(1')	−40 (4)†	5209 (1)	3277 (0)
O(1)	3542 (19)	2199 (20)	4848 (6)*
O(1')	2729 (20)	−2975 (18)	5152 (6)*
O(2)	2789 (50)	2385 (32)	2502 (17)
O(2')	2877 (49)	7614 (33)	7493 (17)
O(3)	977 (30)	668 (35)	6087 (4)*
O(3')	890 (33)	−504 (35)	3913 (4)*

* These parameters were constrained to have no *Cmma* component.

† Used to fix origin in $P2_1ab$.

Table 5. U_{ij} *thermal parameters for* Bi_2WO_6

The thermal parameters of atoms X and X' related by the pseudo 2_x symmetry axis were constrained so that $U_{ij} = U_{ij}'$ for $ij =$ 11,22,33,23 and $U_{ij} = -U_{ij}'$ for $ij = 12,13$. Values are times 10^{-3} Å^2.

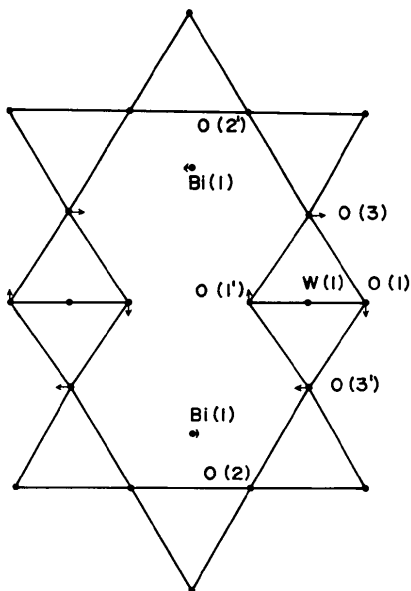|	U_{11}	U_{22}	U_{33}	U_{12}	U_{13}	U_{23}	$\langle U \rangle$
W(1)	5 (0)	3 (0)	5 (0)	0 (−)	0 (−)	0 (0)	4 (0)
Bi(1)	9 (0)	8 (0)	8 (0)	−1 (0)	2 (0)	1 (0)	8 (0)
Bi(1')	9 (0)	8 (0)	8 (0)	1 (−)	−2 (−)	1 (0)	8 (0)
O(1)	7 (2)	7 (0)	15 (5)	1 (0)	3 (0)	−4 (0)	10 (2)
O(1')	7 (2)	7 (2)	15 (5)	−1 (2)	−3 (2)	−4 (2)	10 (2)
O(2)	8 (3)	8 (1)	10 (3)	2 (1)	3 (2)	1 (2)	9 (1)
O(2')	8 (3)	8 (1)	10 (3)	−2 (2)	−3 (2)	1 (2)	9 (1)
O(3)	9 (3)	8 (1)	17 (4)	2 (1)	−2 (1)	−3 (1)	12 (1)
O(3')	9 (3)	8 (1)	17 (4)	−2 (1)	2 (2)	−3 (1)	12 (1)

Fig. 5. A section of the *Fmmm* parent structure projected down **a**. The superimposed arrows correspond to the *Bmab* component of the atom displacements (see Table 6). The other section per unit cell is displaced by (**a** + **b**)/2 and is not shown for clarity. The arrows are reversed for this other section. Only atoms between $\frac{1}{4}c$ and $\frac{3}{4}c$ are shown. The remaining atoms are related by *B*-centering.

Table 6. *Displacive components for the displacive modes of* Bi_2WO_6

Displacements are given as fractions of unit-cell dimensions ($\times 10^4$). The total displacement for an atom is the sum of the components.

| | F2mm | | Bmab | | Abam | | Amam | | Ccma | | Bhab | | Cmma |
	Δx	Δy	Δy	Δz	Δx	Δy	Δy	Δz	Δx	Δy	Δy		Δz
W(1)	209						79						0*
Bi(1)	0†	−200					9		40				0*
Bi(1')	0†	200					9		−40				0*
O(1)	635	87			−152	406	−388						0*
O(1')	635	−87			152	−406	388						0*
O(2)	333		4			0		−2	−44	−114			
O(2')	333		−4			0		−2	44	114			
O(3)	933		586				82		44				0*
O(3')	933		−586				82		−44				0*

* Constrained to be 0.

† Origin fixing in $P2_1ab$.

Table 7. *Geometry of the* W *and* Bi *environments in* Bi_2WO_6

Distances (Å)

Distances <4.0 Å are listed for the Bi atoms. Distances and angles <2.2 Å are listed for the W atom. Distances in the same row of the table would be equivalent in the *Fmmm* parent structure. O atoms are coded to indicate what special position of *Fmmm* they have been displaced from, *viz.* $(a) -\frac{1}{4}$, $\frac{1}{4}$, z; $(b) -\frac{1}{4}$, $\frac{3}{4}$, z; $(c)\frac{1}{4}$, $\frac{1}{4}$, z; $(d)\frac{1}{4}$, $\frac{3}{4}$, z; $(e) -\frac{1}{4}$, $\frac{1}{4}$, z; (f) 0, 0, z; (g) 0, 1, z; $(h)\frac{1}{4}$, $\frac{1}{4}$, z; (i) 0, $\frac{1}{4}$, z; $(j)\frac{1}{4}$, $\frac{3}{4}$, z; $(k)\frac{3}{4}$, $\frac{1}{4}$, z; $(l)\frac{3}{4}$, $\frac{3}{4}$, z; $(m)\frac{3}{4}$, $\frac{1}{4}$, z; (n) 1, 1, z; (o) 1, 0, z; $(p)\frac{3}{4}$, $\frac{1}{4}$, z; (q) 1, $\frac{1}{4}$, z; $(r) -\frac{1}{4}$, $-\frac{1}{4}$, z; (s) 0, 0, $1-z$; $(t)\frac{1}{4}$, $-\frac{1}{4}$, z.

Bi(1)—O(2')a 2·188 (25) —O(2')b 2·226 (23) —O(2')c 2·341 (26) —O(2')d 2·514 (23)
  —O(3)e 2·464 (15) —O(3)f 2·534 (18) —O(3)g 3·390 (18) —O(3)h 3·413 (16)
  —O(3)i 3·664 (8)
  —O(1')d 3·204 (10) —O(1')b 3·348 (9) —O(1)a 3·369 (9) —O(1)c 3·893 (10)
Bi(1')—O(2)j 2·180 (25) —O(2)k 2·239 (24) —O(2)l 2·328 (26) —O(2)m 2·522 (24)
  —O(3')h 2·459 (17) —O(3')n 2·604 (18) —O(3')o 3·316 (18) —O(3')p 3·404 (17)
  —O(3')q 3·654 (8)
  —O(1)k 2·996 (9) —O(1')l 3·570 (9) —O(1)m 3·628 (10) —O(1')j 3·638 (9)
W(1)—O(1)a 1·755 (11) —O(1)r 2·167 (10) —O(1')f 1·789 (10) —O(1')s 2·170 (10)
  —O(3')c 1·851 (8) —O(3)t 1·862 (8)

O—W(1)—O angles (°)

O(1)c	O(1')r	172·1 (5)	O(1')t	O(1)a	171·9 (5)	O(3)s	O(3')f	155·4 (4)
O(1)c	O(1')t	83·6 (5)	O(1)c	O(3)s	80·2 (5)	O(1)c	O(3')f	79·2 (6)
O(1)c	O(1)a	88·3 (2)	O(1')t	O(3)s	83·0 (6)	O(1')t	O(3')f	81·5 (6)
O(1')t	O(1')r	100·2 (6)	O(3)s	O(1')r	98·4 (6)	O(3)s	O(1)a	96·2 (6)
O(3')f	O(1')r	100·2 (6)	O(3')f	O(1)a	96·4 (6)	O(1')r	O(1)a	99·6 (6)

Fig. 6). The mean displacement of the octahedron oxygen framework, atoms O(1), O(1'), O(3), O(3'), from the parent along the **a** axis is 0·43 Å, which is comparable with the other re-refined structures. The W atom is displaced only 0·12 Å in the same direction, which implies that it is displaced 0·32 Å relative to the centre of the octahedron. Therefore, of all the MO_6 octahedra observed in the three structures refined to date, the W in WO_6 is furthest displaced from the centre of the octahedron. A full comparison of the re-refined structures and a discussion of the chemistry of $Bi_4Ti_3O_{12}$, Bi_3TiNbO_9 and Bi_2WO_6 is published elsewhere (Withers, Thompson & Rae, 1991).

We have calculated the dipole moment per unit volume of Bi_2WO_6 using ionic species Bi^{3+}, W^{6+} and O^{2-} and obtained 46 μC cm^{-2}. This compares with

42 μC cm^{-2} calculated by Wolfe, Newnham & Kay, (1969) for their refined model. We are unaware of any experimental value for this material.

While we have described Bi_2WO_6 in terms of a commensurate modulation of an idealized *Fmmm* parent structure derived from an *I4/mmm* structure, it is not necessary for these purposes that this structure actually exists, even though such high-symmetry polymorphs do exist above T_c for other Aurivillius phases *e.g.* $Bi_4Ti_3O_{12}$. Reversible phase transitions
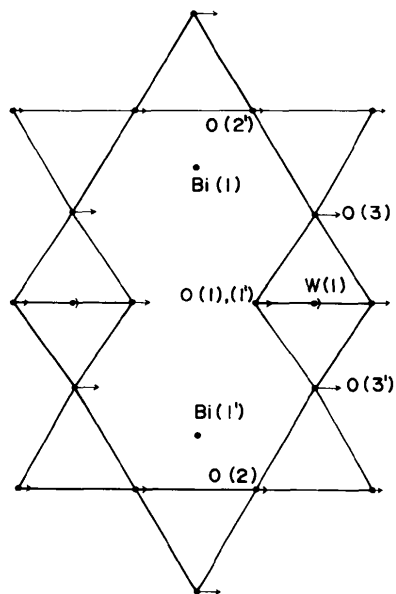
Fig. 6. A section of the *Fmmm* parent structure projected down **b**. The superimposed arrows correspond to the *F2mm* component of the atom displacements (see Table 6). The other section per unit cell is displaced by (**a** + **b**)/2 and is not shown. Only atoms between ¼c and ¾c are shown. The remaining atoms are related by *B*-centering. The *F2mm* component corresponds to the spontaneous polarization along **a**.
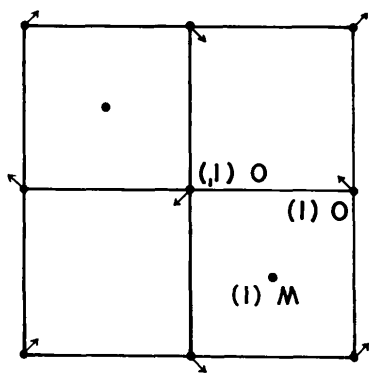

Fig. 7. The *Abam* displacive mode showing the 90° rotation of WO_6 octahedra about axes parallel to **c**. This mode can be either *A*-centred (*Abam* symmetry) or *B*-centred (*Bbam* symmetry). The majority component has *Abam* symmetry.

Table 8. *Apparent valences for atoms in* Bi_2WO_6

	Parent	F2mm	Bmab	Abam	2Mode[a]	3Mode[b]	Total[c]	Wolfe[d]
Bi(1)	2·79	3·02	2·95	2·80	3·16	3·16	3·18	2·96
Bi(1')	2·79	3·02	2·95	2·80	3·16	3·18	3·16	2·96
W(1)	6·46	6·65	6·10	6·22	6·30	6·04	6·06	6·72
O(1)	1·98	2·22	1·91	1·87	2·14	1·95	2·11	2·30
O(1')	1·98	2·22	1·91	1·87	2·14	2·09	1·95	2·30
O(2)	2·23	2·29	2·25	2·23	2·32	2·32	2·31	2·25
O(2')	2·23	2·29	2·25	2·23	2·32	2·32	2·31	2·25
O(3)	1·81	1·83	1·84	1·81	1·85	1·85	1·86	1·77
O(3')	1·81	1·83	1·84	1·81	1·85	1·85	1·85	1·77

Notes: (*a*) The sum of *F2mm* and *Bmab* displacements. (*b*) The sum of *F2mm*, *Bmab* and *Abam* displacements. (*c*) The sum of all modes, the final refined structure. (*d*) The refined structure of Wolfe *et al.* (1969).

have been reported for Bi_2WO_6 at 935 and 1235 K (Watanabe, 1982) which would be consistent with a progressive raising of symmetry. However, there is no evidence to date to confirm the existence of a tetragonal form of Bi_2WO_6 above ~1235 K. Rather, high-temperature XRD studies have indicated a sizeable volume change at this temperature consistent with a reconstructive phase transition, giving a high-temperature polymorph with monoclinic symmetry (Watanabe, 1982; Yanovskii, Voronkova & Milyutin, 1983). There is, however, a significant lack of agreement among various authors as to the structure or even existence of this 'monoclinic' phase (Newkirk, Quadflieg, Liebertz & Kockel, 1972; Watanabe, 1982; Yanovskii, Voronkova & Milyutin, 1983).

Crystal chemistry

As in our recent refinements of $Bi_4Ti_3O_{12}$ (Rae, Thompson, Withers & Willis, 1990) and Bi_3TiNbO_9 (Thompson, Rae, Withers & Craig, 1991) we have calculated apparent valences (AV's) to confirm the chemical plausibility of the refined structure and to help understand the driving force underlying the various observed displacive modes (Table 8).

In common with the parent $Bi_4Ti_3O_{12}$ and Bi_3TiNbO_9 structures, the AV's of the perovskite *B* atom, in this case W, and the Bi atom in the Bi_2O_2 layer are overbonded and underbonded, respectively. The octahedral rotation modes, *Bmab* and *Abam*, again serve to reduce the overbonding of the perovskite *B* atom, effectively by increasing the dimensions of the octahedron of oxygen atoms. However, it is the 'ferroelectric' *F2mm* mode which principally corrects for the underbonding of the Bi_2O_2 layer Bi atom.

Also in common with the previous refined structures, the oxygen atoms on either side of the Bi_2O_2 layer Bi atom, O(2) and O(3), appeared to be overbonded and underbonded, respectively, while the Bi atom in between appears to be satisfactorily bonded. Given the internal consistency of this feature among

the, now, three independently re-refined structures, we must conclude that this feature is normal for this structure type and arises from the inability of the apparent valence method to handle atoms possessing lone pairs in highly anisotropic structural environments, such as Bi^{3+} in the Bi_2O_2 layer of Aurivillius phases.

In all of our previous calculations of AV's we have used the empirical parameters derived by Brown & Altermatt (1985). For the present calculations we retained their values of $r_0 = 2.094$ Å for Bi^{3+}—O^{2-} but did not use their value of $r_0 = 1.917$ Å for W^{6+}—O^{2-} for reasons discussed by Domenges, McGuire & O'Keeffe (1985). Instead we used $r_0 = 1.900$ Å which we derived from simple perovskite-related W^{VI} containing oxides.

References

ALCOCK, N. W. (1970). *Acta Cryst.* A26, 437–439.
BRADLEY, C. J. & CRACKNELL, A. P. (1972). *The Mathematical Theory of Symmetry in Solids. Representation Theory for Point Groups and Space Groups.* Oxford: Clarendon Press.
BROWN, I. D. (1978). *Chem. Soc. Rev.* 7, 359–376.
BROWN, I. D. (1981). *Structure and Bonding in Crystals*, Vol. II, edited by M. O'KEEFFE & A. NAVROTSKY, pp. 1–30. New York: Academic Press.
BROWN, I. D. & ALTERMATT, D. (1985). *Acta Cryst.* B41, 244–247.
COPPENS, P. & HAMILTON, W. C. (1970). *Acta Cryst.* A26, 71–83.
DOMENGES, B., McGUIRE, N. K. & O'KEEFFE, M. (1985). *J. Solid State Chem.* 56, 94–100.
DORRIAN, J. F., NEWNHAM, R. E., SMITH, T. K. & KAY, M. I. (1971). *Ferroelectrics*, 3, 17–27.
MEULENAER, J. DE & TOMPA, H. (1965). *Acta Cryst.* 19, 1014–1018.
NEWKIRK, H. W., QUADFLIEG, P., LIEBERTZ, J. & KOCKEL, A. (1972). *Ferroelectrics*, 4, 51–55.
NEWNHAM, R. E., WOLFE, R. W., HORSEY, R. S., DIAZ-COLON, F. A. & KAY, M. I. (1973). *Mater. Res. Bull.* 8, 1183–1195.
RAE, A. D. (1989). *RAELS89. A Comprehensive Constrained Least-Squares Refinement Program.* Univ. of New South Wales, Australia.
RAE, A. D., THOMPSON, J. G. & WITHERS, R. L. (1990). *Acta Cryst.* A46(Suppl.), C-278–C-279.
RAE, A. D., THOMPSON, J. G., WITHERS, R. L. & WILLIS, A. C. (1990). *Acta Cryst.* B46, 474–487.
SHELDRICK, G. M. (1976). *SHELX76.* Program for crystal structure determination. Univ. of Cambridge, England.
THOMPSON, J. G., RAE, A. D., WITHERS, R. L. & CRAIG, D. C. (1991). *Acta Cryst.* B47, 174–180.
WATANABE, A. (1982). *J. Solid State Chem.* 41, 160–165.
WITHERS, R. L., THOMPSON, J. G. & RAE, A. D. (1991). *J. Solid State Chem.* In the press.
WOLFE, R. W., NEWNHAM, R. E. & KAY, M. I. (1969). *Solid State Commun.* 7, 1797–1801.
WOLFE, R. W., NEWNHAM, R. E., SMITH, T. K. & KAY, M. I. (1971). *Ferroelectrics*, 3, 1–7.
YANOVSKII, V., VORONKOVA, V. & MILYUTIN, V. (1983). *Kristallografiya*, 28, 316–319.

Neutron Powder Investigation of the Tetragonal to Monoclinic Phase Transformation in Undoped Zirconia

BY H. BOYSEN AND F. FREY

Institut für Kristallographie und Mineralogie, LMU München, Theresienstrasse 41, 8000 München 2, Germany

AND T. VOGT

Institut Laue–Langevin, BP 156, 38042 Grenoble CEDEX, France

Abstract

The tetragonal (t) to monoclinic (m) transformation in pure ZrO_2 was investigated by neutron powder diffraction at temperatures between 1900 K and room temperature. The results of a Rietveld analysis are compared with a previous investigation of the $m \rightarrow t$ transformation. The $t \rightarrow m$ transformation takes place near 1200 K (implying a hysteresis of 300 K) and in a much smaller interval (about 150 K compared with about 600 K in the $m \rightarrow t$ case). There are no indications of a two-stage process as found for the $m \rightarrow t$ transformation. The structural parameters of the m phase depend only on temperature while those of the t phase differ at the same temperatures for the forward and reverse transformation. The temperature dependence of the lattice constants suggests an orientational relationship $\mathbf{a}_t \| \mathbf{a}_m^*$ and $\mathbf{c}_t \| \mathbf{b}_m$.